quent analysis on a personal computer. In this study, no patient received additional administration of the contrast agent. All of the procedures were performed by one of two skilled investigators with at least 3 years' experience in using CEUS.

2.3. Image analysis

Baseline gray-scale ultrasound and CEUS images were displayed retrospectively from digital video files on a computer screen and evaluated in consensus by two investigators who were not involved in the ultrasound scanning and were unaware of the clinical and other imaging information of patients. The reviewers determined the diameters and echogenicity of the lesions on gray-scale ultrasound and evaluated the time of initial lesion enhancement, enhancement level, and pattern of each lesion at different phases of CEUS. The level of enhancement was divided into nonenhancing, hypoenhancing, isoenhancing, and hyperenhancing, according to the peak enhancement of lesion compared with the surrounding liver parenchyma. Contrast enhancement patterns were classified as homogenous, heterogeneous, rim, and peripheral nodular enhancement.

3. Results

3.1. HCC

On baseline gray-scale ultrasound, all HCCs were heterogeneously hypoechoic, with ovoid shape and sharp margins. After injection of the UCA, initial enhancement in all lesions appeared earlier than the initial enhancement of the liver parenchyma in the arterial phase of CEUS. There were eight (80%) lesions with homogeneous enhancement and two (20%) lesions with heterogeneous enhancement (Table 2). As to the enhancement level, all lesions exhibited hyperenhancement in the arterial phase. In the portal phase, all lesions demonstrated contrast enhancement washout and became hypoenhanced in eight (80%) patients and isoenhanced in two (20%) patients. In the late phase, all lesions were hypoenhancing compared with the surrounding liver parenchyma (Table 3).

When homogeneous or heterogeneous hyperenhancement in the arterial phase (with washout of contrast enhancement in the portal and late phases) was regarded as a positive finding of HCC, the sensitivity, specificity, positive predictive value (PPV), negative predictive value (NPV), and accuracy of real-time CEUS were found to be 100% (10 of 10), 95.6% (86 of 90), 71.4% (10 of 14), 100% (86 of 86), and 96% (96 of 100), respectively (Table 4).

3.2. MLC

MLCs were heterogeneously hyperechoic in two (40%) patients and hypoechoic in three (60%) patients on baseline gray-scale ultrasound. All lesions were ovoid in shape, with sharp margins. In the arterial phase of CEUS, all lesions enhanced earlier than the liver parenchyma. There were two (40%) lesions with homogeneous enhancement and three (60%) lesions with rim enhancement. As to the enhancement level, all lesions exhibited hyperenhancement in the arterial phase and hypoenhancement in the portal and late phases in relation to the surrounding liver parenchyma (Fig. 1).

When rim hyperenhancement in the arterial phase (with washout of contrast enhancement in the portal and late phases) was regarded as a positive finding of MLC, the sensitivity, specificity, PPV, NPV, and accuracy of real-time CEUS were found to be 60% (3 of 5), 100% (95 of 95), 100% (3 of 3), 97.9% (95 of 97), and 98% (98 of 100), respectively.

3.3. ICC

On baseline gray-scale ultrasound, both ICCs appeared to be heterogeneously hypoechoic, with ovoid shape and sharp margins. On CEUS images, both lesions showed heterogeneous hyperenhancement in the arterial phase, with one earlier emergence and one simultaneous emergence of enhancement when compared with the adjacent liver parenchyma. Both lesions appeared to be hypoenhancing in the portal and late phases and were misdiagnosed as HCC in the present study (Fig. 2).

Table 2
Enhancement patterns of FLLs in the arterial phase (N=100)

Pattern	Homogeneous enhancement	Heterogeneous enhancement	Peripheral nodular enhancement	Rim-like enhancement	No enhancement
HCC	8 (80)	2 (20)	–	–	–
ICC	–	2 (100)	–	–	–
MLC	2 (40)	–	–	3 (60)	–
Hemangioma	1 (3.3)	1 (3.3)	28 (93.4)	–	–
FNH	8 (100)	–	–	–	–
Focal fatty sparing lesions	40 (95.2)	–	–	–	2 (4.8)
Abscess	–	–	–	2 (100)	–
SNN	–	–	–	–	1 (100)

Data are numbers of lesions; data in parentheses are percentages.

Table 3
Enhancement levels of FLLs in different vascular phases (N=100)

Enhancement level	Arterial phase				Portal phase				Late phase			
	Hyper	Iso	Hypo	No	Hyper	Iso	Hypo	No	Hyper	Iso	Hypo	No
HCC	10 (100)	–	–	–	–	2 (20)	8 (80)	–	–	–	10 (100)	–
ICC	2 (100)	–	–	–	–	–	2 (100)	–	–	–	2 (100)	–
MLC	5 (100)	–	–	–	–	–	5 (100)	–	–	–	5 (100)	–
Hemangioma	30 (100)	–	–	–	28 (93.3)	2 (6.7)	–	–	27 (90)	2 (6.7)	1 (3.3)	–
FNH	8 (100)	–	–	–	3 (37.5)	5 (72.5)	–	–	3 (37.5)	4 (50)	1 (12.5)	–
Focal fatty sparing lesions	–	40 (95.2)	–	2 (4.8)	–	40 (95.2)	–	2 (4.8)	–	39 (92.9)	1 (2.3)	2 (4.8)
Abscess	2 (100)	–	–	–	–	–	2 (100)	–	–	–	2 (100)	–
SNN	–	–	–	1 (100)	–	–	–	1 (100)	–	–	–	1 (100)

Note. Data are numbers of lesions; data in parentheses are percentages.

3.4. Hemangioma

Apart from 3 (10%) hyperechoic lesions, 27 (90%) hemangiomas were heterogeneously hypoechoic, with round shape and sharp margins on baseline gray-scale ultrasound. After injection of the UCA, enhancement of lesions appeared earlier than enhancement of the liver parenchyma in 28 (93.3%) lesions and appeared simultaneously with enhancement of the liver parenchyma in 2 (6.7%) lesions. There were 28 (93.3%) lesions with peripheral nodular enhancement with progressive centripetal fill-in, 1 (3.3%) lesion with homogeneous enhancement, and 1 (3.3%) lesion with heterogeneous centrifugal radiating enhancement. As to the enhancement level, all lesions exhibited hyperenhancement in the arterial phase. In the late phase, 27 (90%) lesions remained hyperenhanced, 2 (6.7%) lesions washed out to isoenhancement, and 1 (3.3%) lesion washed out to hypoenhancement with respect to the surrounding liver parenchyma (Fig. 3).

When peripheral nodular enhancement with progressive centripetal fill-in in the arterial phase (with or without washout of contrast agent in the portal and late phases) was regarded as a positive finding of hemangioma, the sensitivity, specificity, PPV, NPV, and accuracy of real-time CEUS were found to be 93.3% (28 of 30), 98.6% (69 of 70), 96.6% (28 of 29), 97.2% (69 of 71), and 97% (97 of 100), respectively.

3.5. FNH

All FNHs were heterogeneously hypoechoic, with round shape and sharp margins on baseline gray-scale ultrasound. No wheel-like blood vessels were depicted by color Doppler ultrasound. On CEUS, all lesions showed homogeneous hyperenhancement, with earlier time of initial enhancement compared to the liver parenchyma. There were seven (87.5%) lesions with centrifugal radiating enhancement and one (12.5%) lesion with immediately homogeneous enhancement. Wheel-like feeding arteries were shown in four (50%) lesions at the beginning of the arterial phase. No central scar was shown on CEUS imaging in the present study. As to the enhancement level, all lesions exhibited hyperenhancement in the arterial phase, and three (37.5%) of them remained hyperenhanced in the portal and late phases. Five (62.5%) lesions washed out to isoenhancement in the portal phase, and only one (12.5%) lesion appeared as hypoenhancement in the late phase with respect to the surrounding liver parenchyma (Fig. 4).

When centrifugal radiating hyperenhancement, combined with wheel-like feeding blood vessels in the arterial phase (with or without washout of contrast agent in the portal and late phases), was regarded as a positive finding of FNH, the sensitivity, specificity, PPV, NPV, and accuracy of real-time CEUS were found to be 87.5% (7

Table 4
Diagnostic performance of CEUS in different FLLs in fatty liver

Entity	Sensitivity	Specificity	PPV	NPV	Accuracy
HCC	100% (10 of 10)	95.6% (86 of 90)	71.4% (10 of 14)	100% (86 of 86)	96% (96 of 100)
MLC	60% (3 of 5)	100% (95 of 95)	100% (3 of 3)	97.9% (95 of 97)	98% (98 of 100)
ICC	0% (0 of 2)	100% (98 of 98)	NA	98% (98 of 100)	98% (98 of 100)
Hemangioma	93.3% (28 of 30)	98.6% (69 of 70)	96.6% (28 of 29)	97.2% (69 of 71)	97% (97 of 100)
FNH	87.5% (7 of 8)	97.8% (90 of 92)	77.8% (7 of 9)	98.9% (90 of 91)	97% (97 of 100)
Focal fatty sparing lesions	92.6% (39 of 42)	100% (58 of 58)	100% (39 of 39)	95.1% (58 of 61)	97% (97 of 100)
Abscess	100% (2 of 2)	100% (98 of 98)	100% (2 of 2)	100% (98 of 98)	100% (100 of 100)
SNN	100% (1 of 1)	98.0% (97 of 99)	33.3% (1 of 3)	100% (97 of 97)	98% (98 of 100)

Numbers in parentheses are the numbers of lesions used to calculate percentages.
NA, not applicable.

of 8), 97.8% (90 of 92), 77.8% (7 of 9), 98.9% (90 of 91), and 97% (97 of 100), respectively.

3.6. Focal fatty sparing lesions

All of the 42 focal fatty sparing lesions were homogeneously hypoechoic, with round shape and sharp margins on baseline gray-scale ultrasound. Except for 2 (4.8%) lesions with no obvious enhancement (Fig. 5), the remaining 40 (95.2%) lesions showed homogeneous isoenhancement during the arterial and portal phases of CEUS. Only one lesion washed out to hypoenhancement with respect to the surrounding liver parenchyma at 4 min after UCA administration.

When homogeneous isoenhancement during the vascular phase was regarded as a positive finding of focal fatty sparing lesions, the sensitivity, specificity, PPV, NPV, and accuracy of real-time CEUS were found to be 92.6% (39 of 42), 100% (58 of 58), 100% (39 of 39), 95.1% (58 of 61), and 97% (97 of 100), respectively.

3.7. Pyogenic hepatic abscess

On baseline gray-scale ultrasound, both abscesses were heterogeneously hypoechoic, with a central anechoic area and irregular margins. CEUS showed irregular rim enhancement with nonenhanced areas and enhanced septa inside lesions. No transient hyperenhanced liver parenchyma around lesions was depicted in the early arterial phase. As to the enhancement level, both lesions exhibited hyperenhancement in the arterial phase and hypoenhancement in the portal and late phases. Both lesions were correctly characterized as abscess because of specific enhancement patterns.

3.8. SNN

The solitary lesion appeared homogeneously hypoechoic, with round shape and sharp margins on baseline gray-scale ultrasound. After administration, the lesion showed no enhancement during the vascular phases of

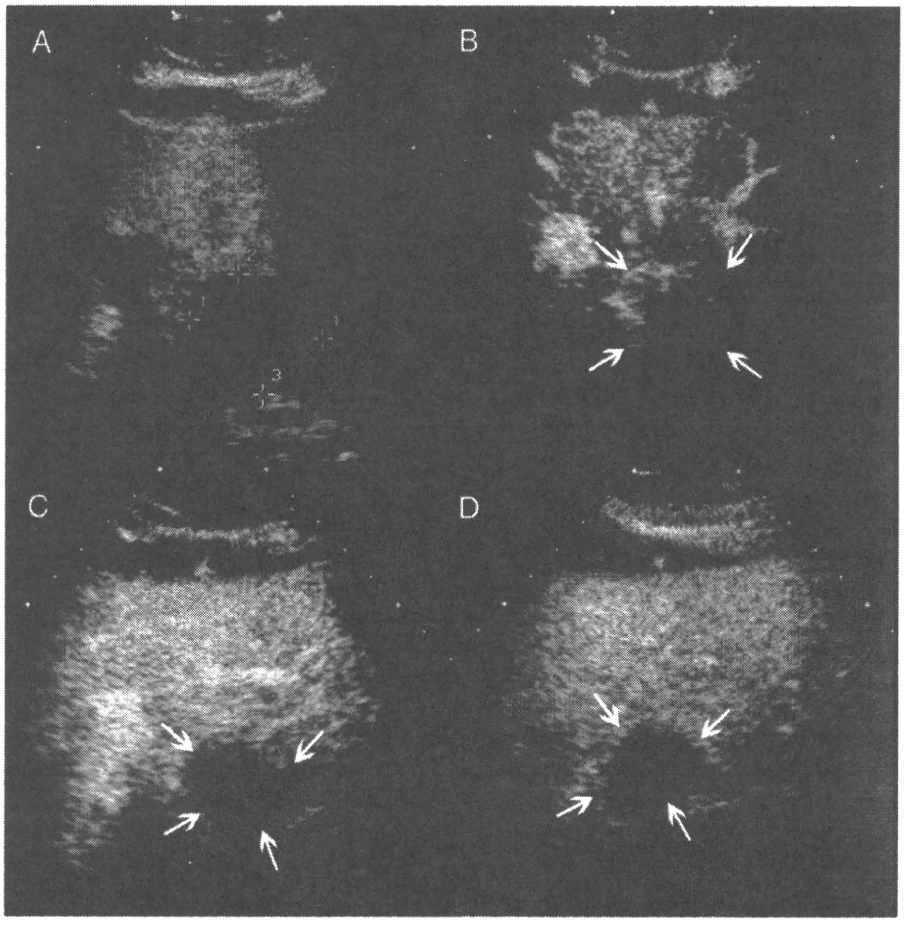

Fig. 1. A 59-year-old female patient with liver metastasis from breast carcinoma. (A) Baseline ultrasound image shows a hypoechoic lesion (3.5 cm in diameter) in Segment III of the liver. (B) Arterial-phase image obtained 22 s after contrast agent administration shows rim hyperenhancement of the lesion (arrow). (C) The lesion is hypoenhanced (arrow) compared with the surrounding liver parenchyma in the portal phase (52 s). (D) Late-phase image (180 s) shows complete washout of contrast agents (arrow).

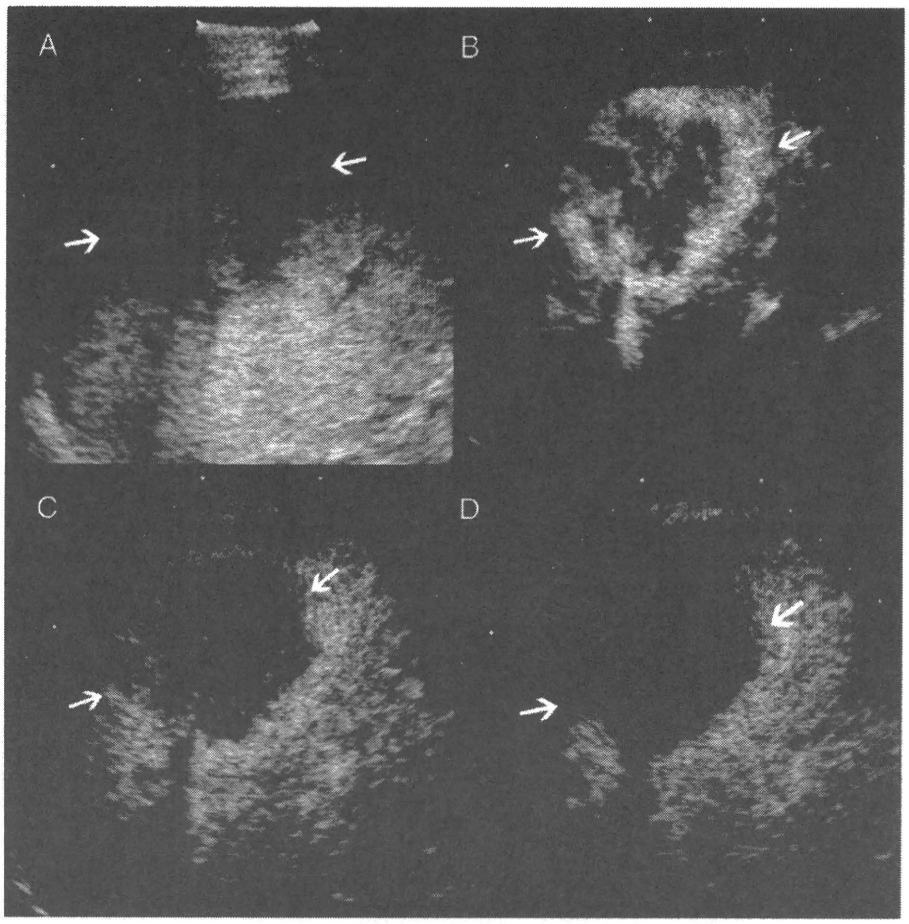

Fig. 2. A 52-year-old male patient with ICC. (A) Baseline ultrasound image shows a hypoechoic lesion (5.8 cm in diameter) in Segment VII of the liver. (B) Arterial-phase image obtained 22 s after contrast agent administration shows heterogeneous hyperenhancement of the lesion. (C) The lesion appears to be hypoenhancement with respect to the surrounding liver in the portal phase (50 s). (D) Late-phase image (150 s) shows complete washout of the contrast enhancement of the lesion.

CEUS. We made the correct diagnosis of SNN according to CEUS findings.

4. Discussion

FLLs on diffuse liver disease background are quite common on clinical ultrasound examination. Although the presence of liver cirrhosis may alter the sonographic appearance of FLLs, it is also an important diagnostic clue for radiologists in their diagnosis of HCC or regeneration of nodules. Hepatic steatosis will not only make the characterization of FLLs more difficult by increasing parenchyma echogenicity and altering the typical appearance of the lesion but also make the detection of FLLs insufficient by increasing the attenuation of ultrasound beam and causing poor visualization of the deep areas of the liver [6,7].

The poor diagnostic performance of conventional gray-scale ultrasound in FLLs with diffuse liver disease background has greatly improved with the help of high-MI CEUS [8,9]. Kim et al. [9] reported that the diagnostic performance of high-MI CEUS has greatly improved compared with conventional gray-scale ultrasound after a receiver operating characteristic (ROC) analysis of 75 FLLs in patients with diffuse liver disease (liver cirrhosis in 30, steatosis in 23, chronic hepatitis in 16, and both steatosis and liver cirrhosis in 6). The correctly specific diagnosis

Fig. 3. A 52-year-old male patient with hemangioma. (A) Baseline ultrasound image showed a hypoechoic lesion (7.2 cm in diameter) in Segment VII of the liver. (B) Arterial-phase image obtained 20 s after contrast agent administration shows centrifugal radiating enhancement of the lesion. (C) The lesion is homogeneously hyperenhanced in the portal phase (76 s). (D) The lesion is hypoechoic compared with the surrounding liver parenchyma in the late phase (200 s). (E) Plan CT scan shows a slightly low-attenuation lesion in the right lobe of the liver. (F) There is no obvious enhancement of the lesion on arterial-phase CECT image. (G) Portal-phase image of CECT shows hyperenhancement in the center part of the lesion. (H) The lesion is homogeneously hyperenhanced compared with the surrounding liver parenchyma in the late phase.

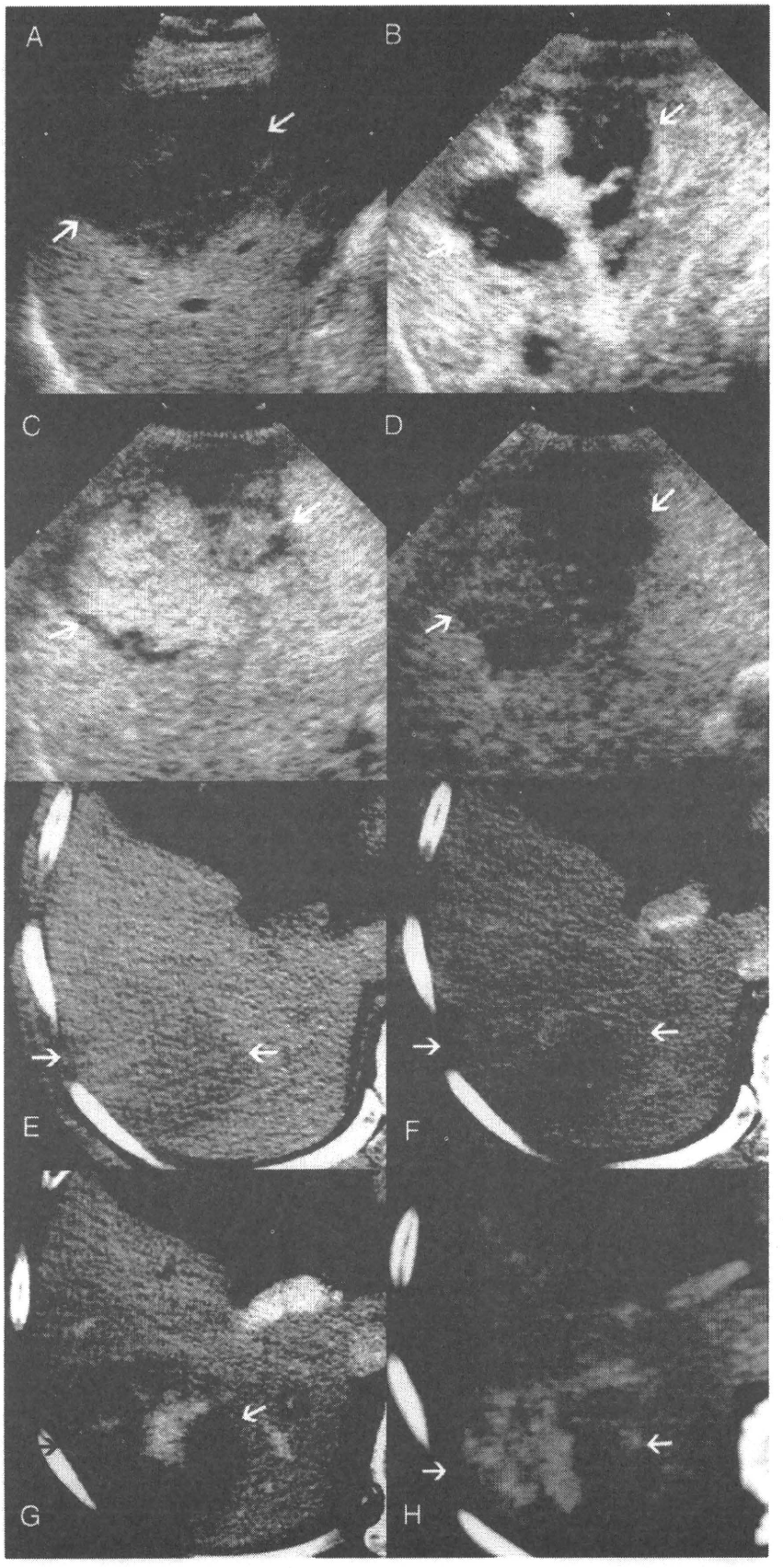
A
B
C
D
E
F
G
H

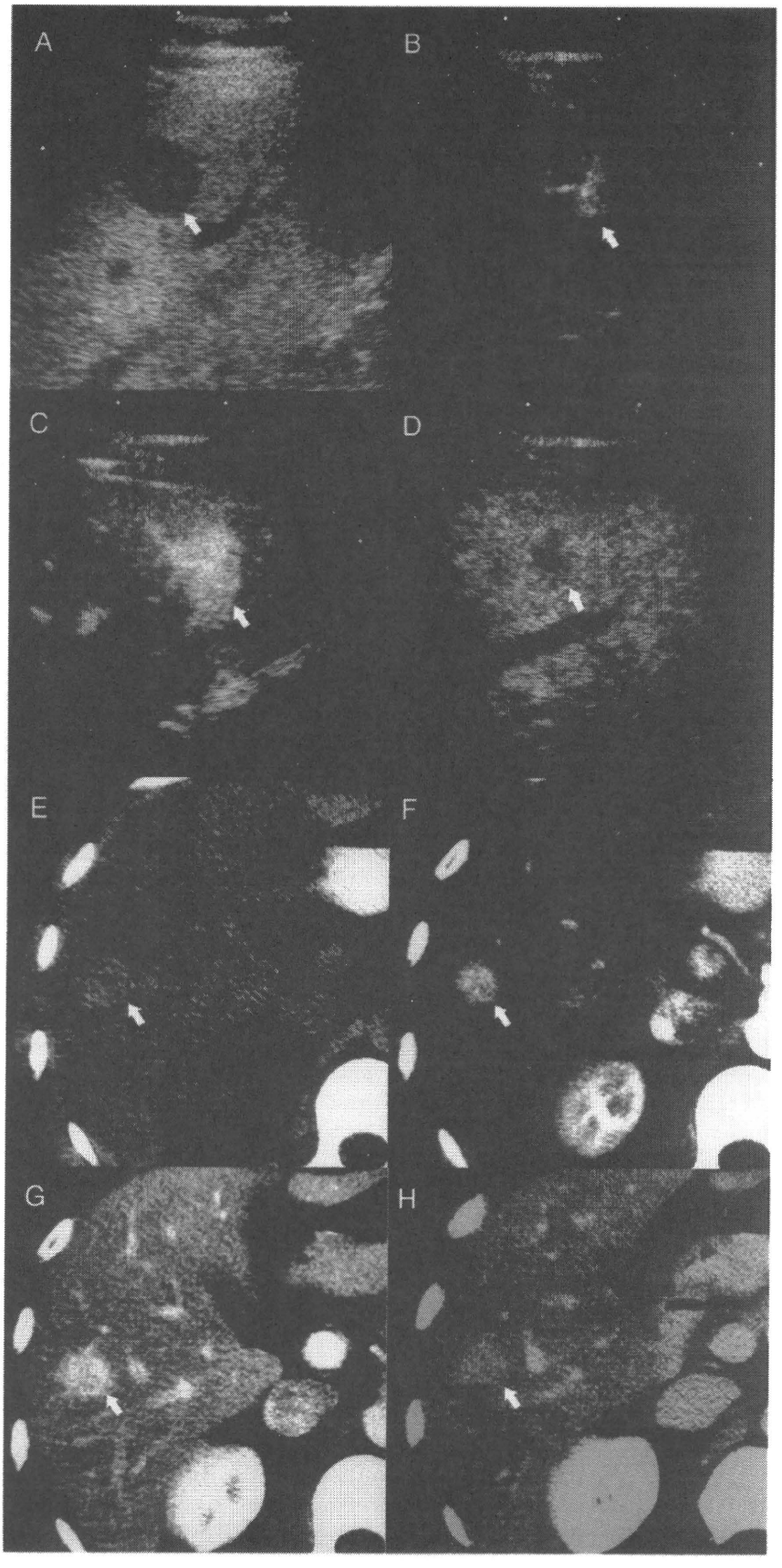
A
B
C
D
E
F
G
H

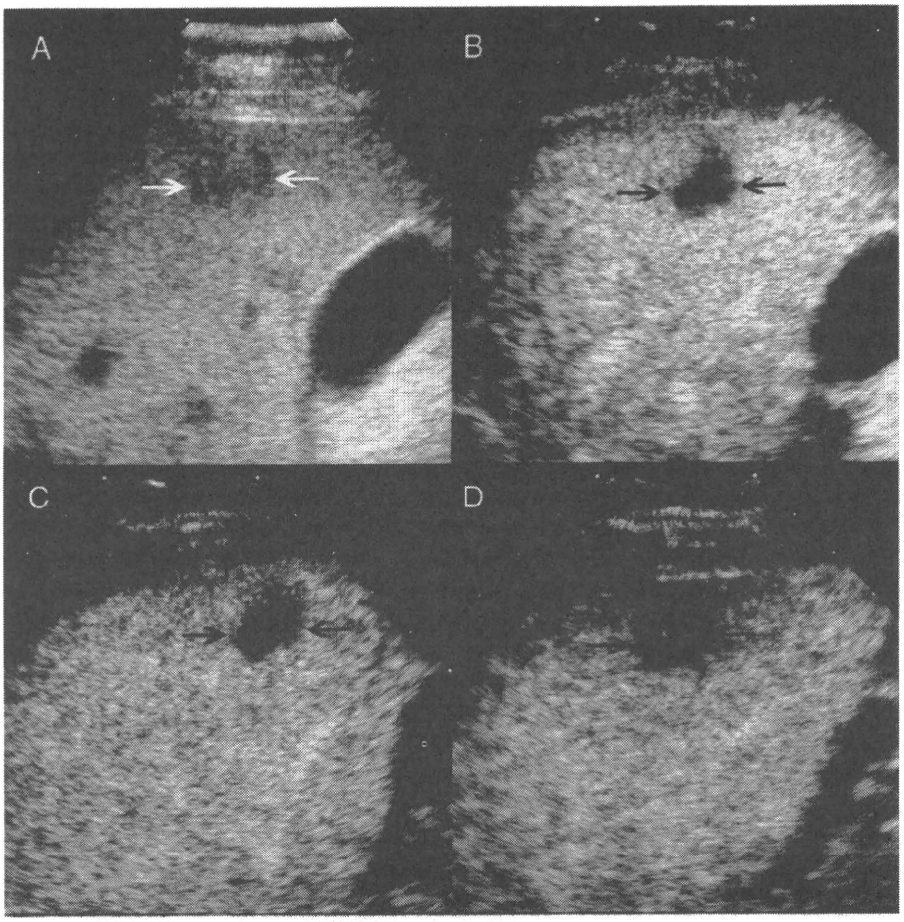

Fig. 5. A 42-year-old male patient with focal fatty sparing lesions. (A) Baseline ultrasound image shows a hypoechoic lesion (2.0 cm in diameter; arrows) in Segment V of the liver. (B–D) The lesion (arrows) shows no obvious enhancement during the vascular phases of CEUS (24, 81, and 168 s after administration of contrast agent).

improved from around 40% on baseline ultrasound to almost 80% on high-MI CEUS.

The newly developed low-MI CEUS techniques using the second generation of UCA showed CEUS more advance than high-MI CEUS in real time and an accurate demonstration of vascularity in FLLs [1]. As expected, satisfactory performance on the characterization of FLLs with real-time CEUS and second-generation UCA has been reported not only in normal liver background but also in fatty liver background [1–5,10]. Bartolotta et al. [10] reported that areas under ROC curves improved from 0.706 for baseline ultrasound to 0.999 for real-time CEUS on 105 FLLs in patients with fatty liver background. The correctly specific diagnosis improved from 28% on baseline ultrasound to 90% on CEUS.

The basic principles of contrast-specific ultrasound techniques are cancellation and/or separation of linear ultrasound signals from tissues and utilization of nonlinear response from UCA microbubbles [1,14]. Even though low-MI contrast-specific techniques may suppress tissue harmonic signals effectively, nonlinear harmonic ultrasound signals may still arise in tissues, especially in deep or fat tissues, and cause an erroneous interpretation of the imaging [1,14,15].

Wilson et al. [15] reported that the CEUS enhancement pattern of some fat-containing FLLs disagreed with CECT/contrast-enhanced MRI findings, which showed hyperechogenicity on CEUS compared with its low attenuation on CT and low signal intensity on MRI. It was presumed that the enhancement caused by the contrast agent is added

Fig. 4. A 29-year-old female patient with FNH. (A) Baseline ultrasound image shows a well-defined hypoechoic lesion (2.2 cm in diameter; arrow) in the right lobe of the liver. (B) Arterial-phase image obtained 10 s after contrast agent administration shows wheel-like blood vessels in the center of the lesion (arrow). (C) Arterial-phase image (17 s) shows homogeneous hyperenhancement of the lesion (arrow). (D) The lesion shows obvious washout of contrast enhancement (arrow) in the late phase (200 s). (E) Plan CT scan shows a slightly high-attenuation lesion in Segment VI of the liver (arrow). (F) Arterial-phase image of CECT shows hyperenhancement of the lesion (arrow). (G) The lesion is hyperenhanced (arrow) compared with the surrounding liver parenchyma in the portal phase. (H) There is no washout of contrast enhancement of the lesion on a late-phase CECT image (arrow).

to the baseline echogenicity of the FLLs containing fat and produced an erroneous interpretation of the level of enhancement of the lesion. On the other hand, it may also be possible that fatty liver background presents some difficulties in the correct interpretation of the level of enhancement on CEUS. Bartolotta et al. [10] reported that three hemangiomas, four FNHs, and four focal fatty sparing lesions in fatty liver appeared to be hypoechoic in the portal and late phases of low-MI CEUS using SonoVue, which should be hyperechoic or isoechoic according to the well-known appearances of benign FLLs on CEUS [1–5]. Lin et al. [16] also reported that three FNHs in fatty liver showed hypoenhancement, while all FNHs with normal liver background showed isoenhancement in the late phase of CEUS. In the present study, one hemangioma, one FNH, and one focal fatty sparing lesion also appeared as hypoenhancement with respect to the surrounding liver parenchyma in the late phase, which maybe an erroneous interpretation caused by the hyperbaseline echogenicity of the fatty liver background.

According to a quantitative study, the signal intensity of fatty liver (15.19±2.90 dB) was significantly higher than that of normal liver (10.91±3.15 dB) on baseline ultrasound. There were no significant differences between the signal intensity of normal liver and the signal intensity of fatty liver at 25 and 60 s after Levovist administration, while the signal intensity of normal liver (20.55±3.58 dB) was statistically higher than that of fatty liver (15.05±3.12 dB) at 120 s after UCA administration, which means that the contrast enhancement of liver parenchyma lasts longer in normal liver than in fatty liver [17]. We presume that fast contrast enhancement washout and harmonic signals from fatty liver parenchyma should be the reasons for the hypoenhancement appearance of some benign FLLs in the late phase.

Since the enhancement level of FLLs in fatty liver may be altered especially in the late phase, it is very important to depend on the enhancement pattern of FLLs for correct characterization. The enhancement patterns of several kinds of FLLs on CEUS are very characteristic and well known by radiologists; specific diagnoses of HCC, FNH, hemangioma, focal fatty infiltration, or sparing and hepatic abscess using CEUS showed a very high accuracy [1–5,18,19]. In the present study, all of the primary malignant FLLs (HCC and ICC) showed homogeneous or heterogeneous enhancement, 40% of MLC lesions showed homogeneous enhancement, and 60% showed typical rim enhancement. As to benign FLLs, 93% of hemangiomas showed a characteristic enhancement pattern (peripheral nodular enhancement) with progressive centripetal fill-in. For FNH, all lesions showed homogeneous hyperenhancement, 88% of FNH lesions showed centrifugal radiating enhancement, and 50% showed typical wheel-like feeding arteries in the arterial phase. Over 95% of focal fatty sparing lesions showed homogeneous isoenhancement during the vascular phases of CEUS. All abscess lesions showed irregular rim enhancement with nonenhanced areas and enhanced septa inside the lesion. The only SNN showed no enhancement during the vascular phase of CEUS. According to specific enhancement patterns on CEUS, we achieved satisfactory results in the characterization of FLLs in fatty liver, with a diagnostic accuracy greater than 96%.

In the present study, 40% of MLC and 100% of ICC lesions were misdiagnosed as HCC because the reviewers were blinded to clinical history and laboratory information. It is well known that homogeneous enhancement and rim-like hyperenhancement in the arterial phase are the two common manifestations of MLC on CEUS, depending on the origin of the primary tumor [1–5]. The latter is specific for liver metastasis, whereas the former is hard to discriminate from the enhancement pattern of HCC. As to ICC, it mainly shows irregular peripheral rim-like or heterogeneous hyperenhancement in the arterial phase and hypoenhancement in the portal and late phases. Although we reported that about 94% of ICCs were correctly characterized by combining baseline and CEUS findings [20], the fatty liver background altered the baseline appearance of the lesion, which made correct characterization difficult in the present study. We believe that the diagnostic ability of CEUS for MLC and ICC will improve with clinical history and laboratory information.

Two focal fatty sparing lesions were misdiagnosed as SNN because of the absence of obvious enhancement during all vascular phases of CEUS, and the other one lesion was undetermined because of atypical baseline ultrasound appearance and contrast washout in the late phase. We consider that the nearly avascular appearance of focal fatty sparing lesions may be attributed to compression from surrounding swollen hepatocytes because of accumulation of triglycerides in hepatocytes [21,22].

We also failed to perform correct characterization of one FNH and two hemangiomas. The FNH and one of the hemangiomas were small in size (less than 2.5 cm in diameter) and showed immediately homogeneous enhancement after administration of UCA. The other hemangioma only showed centrifugal radiating enhancement, which was misdiagnosed as FNH.

One of the limitations of this study was that the final diagnoses of fatty liver and FLLs were not totally confirmed with pathological examination because of ethical concerns. However, we think that the final diagnoses of fatty liver and FLLs in our series should be sufficiently appropriate according to well-established clinical diagnostic criteria based on patient history, laboratory data, multiple imaging findings, and follow-up. The other limitation of this study was that we did not make further analysis of the relationship between the enhancement patterns of FLLs on CEUS and the grade of fatty liver or the location of the lesion, which may also fail CEUS examination in some cases.

In conclusion, CEUS can depict the typical enhancement pattern of FLLs in fatty liver. Although some benign FLLs showed contrast enhancement washout in the late phase of CEUS, correct characterization based on the typical enhancement pattern is possible.

References

[1] Claudon M, Cosgrove D, Albrecht T, et al. Guidelines and good clinical practice recommendations for contrast enhanced ultrasound (CEUS)—update 2008. Ultraschall Med 2008;29:28–44.

[2] Quaia E, Caliada F, Bertolotto M, et al. Characterization of focal liver lesions with contrast-specific US modes and a sulfur hexafluoride-filled microbubble contrast agent: diagnostic performance and confidence. Radiology 2004;232:420–30.

[3] von Herbay A, Vogt C, Willers R, Häussinger D. Real-time imaging with the sonographic contrast agent SonoVue: differentiation between benign and malignant hepatic lesions. J Ultrasound Med 2004;23: 1557–68.

[4] Ding H, Wang WP, Huang BJ, et al. Imaging of focal liver lesions: low-mechanical-index real-time ultrasonography with SonoVue. J Ultrasound Med 2005;24:285–97.

[5] Xu HX, Liu GJ, Lu MD, et al. Characterization of small focal liver lesions using real-time contrast-enhanced sonography: diagnostic performance analysis in 200 patients. J Ultrasound Med 2006;25: 349–61.

[6] Konno K, Ishida H, Sato M, et al. Liver tumors in fatty liver: difficulty in ultrasonographic interpretation. Abdom Imaging 2001;26:487–91.

[7] Jeffrey RB, Ralls PW. The liver. In: Jeffrey RB, Ralls PW, editors. Sonography of the abdomen. New York: Raven Press, 1995. p. 71–170.

[8] Fracanzani AL, Burdick L, Borzio M, et al. Contrast-enhanced Doppler ultrasonography in the diagnosis of hepatocellular carcinoma and premalignant lesions in patients with cirrhosis. Hepatology 2001: 34:1109–12.

[9] Kim SH, Lee JM, Lee JY, et al. Value of contrast-enhanced sonography for the characterization of focal hepatic lesions in patients with diffuse liver disease: receiver operating characteristic analysis. AJR Am J Roentgenol 2005;184:1077–84.

[10] Bartolotta TV, Taibbi A, Galia M, et al. Characterization of hypoechoic focal hepatic lesions in patients with fatty liver: diagnostic performance and confidence of contrast-enhanced ultrasound. Eur Radiol 2007;17:650–61.

[11] Bartolotta TV, Midiri M, Galia M, et al. Characterization of benign hepatic tumors arising in fatty liver with SonoVue and pulse inversion US. Abdom Imaging 2007;32:84–91.

[12] Scatarige JC, Scott WW, Donovan PJ, Siegelman SS, Sanders RC. Fatty infiltration of the liver: ultrasonographic and computed tomographic correlation. J Ultrasound Med 1984;3:9–14.

[13] Jacobs JE, Birnbaum BA, Shapiro MA, et al. Diagnostic criteria for fatty infiltration of the liver on contrast-enhanced helical CT. AJR Am J Roentgenol 1998;171:659–64.

[14] Burns PN. Instrumentation for contrast echocardiography. Echocardiography 2002;19:241–58.

[15] Wilson SR, Kim TK, Jang HJ, Burns PN. Enhancement patterns of focal liver masses: discordance between contrast-enhanced sonography and contrast-enhanced CT and MRI. AJR Am J Roentgenol 2007;189: W7–W12.

[16] Lin LW, Yang JJ, Lin XY, et al. Effect of fatty liver background on contrast-enhanced ultrasonographic appearance of focal nodular hyperplasia. Hepatobiliary Pancreat Dis Int 2007;6:610–5.

[17] Bartolotta TV, Midiri M, Scialpi M, et al. Focal nodular hyperplasia in normal and fatty liver: a qualitative and quantitative evaluation with contrast-enhanced ultrasound. Eur Radiol 2004;14:583–91.

[18] Liu GJ, Lu MD, Xu HX, et al. Real-time contrast-enhanced ultrasound imaging of infected focal liver lesions. J Ultrasound Med 2008;27: 657–66.

[19] Catalano O, Sandomenico F, Raso MM, Siani A. Low mechanical index contrast-enhanced sonographic findings of pyogenic hepatic abscess. AJR Am J Roentgenol 2004;182:447–50.

[20] Xu HX, Lu MD, Liu GJ, et al. Imaging of peripheral cholangiocarcinoma with low-mechanical index contrast-enhanced sonography and SonoVue: initial experience. J Ultrasound Med 2006;25:23–33.

[21] Sherlock S, Dooley J. Nutritional and metabolic liver diseases. In: Sherlock S, Dooley J, editors. Diseases of the liver and biliary system. London: Blackwell Sciences, 1997. p. 427–54.

[22] Veenhuizen JJ, Drackley JK, Richard MJ, et al. Metabolic changes in blood and liver during development and early treatment of experimental fatty liver and ketosis in cows. J Dairy Sci 1991;74: 4238–53.

Computer-aided Diagnosis of Focal Liver Lesions by Use of Physicians' Subjective Classification of Echogenic Patterns in Baseline and Contrast-enhanced Ultrasonography[1]

Katsutoshi Sugimoto, MD, Junji Shiraishi, PhD, Fuminori Moriyasu, MD, Kunio Doi, PhD

Rational and Objectives. To develop a computer-aided diagnostic (CAD) scheme for classifying focal liver lesions (FLLs) by use of physicians' subjective classification of echogenic patterns of FLLs on baseline and contrast-enhanced ultrasonography (US).

Materials and Methods. A total of 137 hepatic lesions in 137 patients were evaluated with B-mode and NC100100 (Sonazoid)-enhanced pulse-inversion US; lesions included 74 hepatocellular carcinomas (HCCs) (23: well-differentiated, 36: moderately differentiated, 15: poorly differentiated HCCs), 33 liver metastases, and 30 liver hemangiomas. Three physicians evaluated single images at B-mode and arterial phases with a cine mode. Physicians were asked to classify each lesion into one of eight B-mode and one of eight enhancement patterns, but did not make a diagnosis. To classify five types of FLLs, we employed a decision tree model with four decision nodes and four artificial neural networks (ANNs). The results of the physicians' pattern classifications were used successively for four different ANNs in making decisions at each of the decision nodes in the decision tree model.

Results. The classification accuracies for the 137 FLLs were 84.8% for metastasis, 93.3% for hemangioma, and 98.6% for all HCCs. In addition, the classification accuracies for histological differentiation types of HCCs were 65.2% for well-differentiated HCC, 41.7% for moderately differentiated HCC, and 80.0% for poorly differentiated HCC.

Conclusions. This CAD scheme has the potential to improve the diagnostic accuracy of liver lesions. However, the accuracy in the histologic differential diagnosis of HCC based on baseline and contrast-enhanced US is still limited.

Key Words. Contrast-enhanced sonography; computer-aided diagnosis; focal liver lesion; Sonazoid.

In the diagnosis of focal liver lesions (FLLs) including hepatocellular carcinoma (HCC), liver metastases, hemangioma, and focal nodular hyperplasia (FNH), contrast-enhanced computed tomography (CT) (1) and magnetic resonance imaging (MRI) (2–4) have been employed more commonly than ultrasonography (US). However, the ultrasonographic equipment is less expensive and can be installed easily compared with CT and MRI. Therefore, US may become more popular in the future, especially in the developing countries. In addition, contrast-enhanced US (CEUS) with pulse-inversion (5) (phase-inversion) imaging techniques has been applied for improvement of the diagnostic accuracy of FLLs. Recently, second-generation ultrasonographic contrast agents, such as DMP 115 (Definity; Lantheus Inc., MA) in Canada and BR 1 (SonoVue; Bracco, Milan, Italy) in Europe and China, have been applied in clinical practice. The agent NC100100 (Sonazoid; GE Healthcare, Oslo, Norway) has become clinically available since January 2007, in Japan ahead of other countries. Although the second-generation ultrasonographic contrast agents have not yet been applied in clinical practice

Acad Radiol 2009; 16:401–411

[1] From the Kurt Rossmann Laboratories for Radiologic Imaging Research, Department of Radiology, The University of Chicago, 5841 S. Maryland Ave., MC 2026, Chicago, IL 60637 (K.S., J.S., K.D.); Department of Gastroenterology and Hepatology, Tokyo Medical University, Tokyo, Japan (K.S., F.M.). Received August 22, 2008; accepted September 24, 2008. **Address correspondence to:** K.S. e-mail: sugimoto@comcast.net

doi:10.1016/j.acra.2008.09.018

for the diagnosis of FLLs in United States, CEUS with these agents are being widely used worldwide.

The problem with US, however, is a disparity in the diagnostic accuracy among institutions. Generally, US strongly depends on subjective aspect of the sonologist, compared to CT and MRI (6). Although this problem has not been so serious in so-called "high-volume centers," where US is used routinely for the diagnosis of FLLs, the diagnostic accuracy in an institution where US is performed infrequently can be poorer than that in a "high-volume center." For reducing this disparity as much as possible, the development of a computer-aided diagnosis (CAD) scheme for the classification of FLLs on CEUS has been attempted (7).

The concept and methodology of CAD to assist physicians in detecting abnormal lesions and improving the classification accuracy of the differential diagnosis have been developed and studied in various radiologic imaging fields (8,9). CAD may be defined as a diagnosis made by physicians who take into account the results of automated computer analysis of medical images. The computer output may be used as a "second opinion" for improving physicians' decision-making and avoiding oversights. In this study, we developed and assessed a CAD scheme for classifying FLLs into liver metastasis, hemangioma, and three histologic differentiation types of HCC using physicians' subjective classifications of echogenic patterns of FLLs on baseline US and CEUS.

MATERIALS AND METHODS

Patient Population

The study was approved by the research ethics board of the Tokyo Medical University, Tokyo, Japan; written informed consent was obtained from each patient for the use of ultrasonographic data for research purposes. Between January 2007 and October 2007, we used conventional US to examine 150 consecutive patients who had hepatic tumors. These patients were recruited at the Tokyo Medical University Hospital. In this study, we excluded patients who were critically ill, were hypersensitive to drugs, and/or had lesions that had been characterized by baseline US (ie, obvious cysts and focal fatty sparings). This study was exempted from the review of the institutional review board at the University of Chicago, because no patient information at this institution was used in this study.

The final diagnosis of the lesions indicated that there were 74 patients with HCC (23 well-differentiated, 36 moderately differentiated, 15 poorly differentiated HCCs), 33 patients with liver metastases (18 colon carcinomas, five gastric carcinomas, two pancreatic carcinomas, two rectal carcinomas, two ovarian carcinomas, two lung carcinomas, one bladder carcinoma, one breast carcinoma), 30 patients with hemangioma, five patients with FNH, three with focal fatty sparings, two with peripheral cholangiocarcinomas, two with dysplastic nodules, and one with an epithelioid hemangioendothelioma. All HCCs, liver metastases, FNH, focal fatty sparings, peripheral cholangiocarcinomas, dysplastic nodules, and epithelioid hemangioendothelioma were diagnosed using histologic examination after surgical resection (10 lesions), or by US-guided biopsy (110 lesions). The degree of cellular differentiation (defined as well-, moderately, or poorly differentiated HCC) was determined according to the International Working Party classification (10). The diagnosis of hemangioma was confirmed using contrast-enhanced CT and/or MRI and by the absence of any changes on follow-up imaging after more than 4 months.

For this study, we excluded five patients with FNH, three patients with focal fatty sparings, two patients with dysplastic nodules, two patients with peripheral cholangiocarcinomas, and one patient with epithelioid hemangioendothelioma because the number of the lesions was small. The 137 remaining patients were enrolled in this study. Of these, 107 patients had solitary focal lesions and 30 had multiple focal lesions. For the patients who had more than one focal lesion, the largest and most conspicuous lesion was evaluated; therefore, 137 hepatic lesions were studied.

With regard to the age distribution for each tumor type, there were no significant differences in the mean age between men and women among the patients with HCC (men, 66.1 ± 10.4 years; women, 74.5 ± 8.1 years), patients with metastases (men, 69.4 ± 9.5 years; women, 66.6 ± 10.3 years), and patients with hemangiomas (men, 54.4 ± 12.5 years; women, 53.0 ± 15.2 years). The size of each of the hepatic tumors was measured during baseline US by a physician (K.S.) who had 8 years of experience in liver ultrasonographic imaging and 5 years of experience in CEUS of the liver. The mean maximum tumor diameter was 25 ± 19 mm among HCCs (18 ± 8 mm among well-differentiated HCCs, 22 ± 17 mm among moderately differentiated HCCs, 41 ± 23 mm among poorly differentiated HCCs), 35 ± 15 mm among metastases, and 28 ± 17 mm among hemangiomas. All ultrasonographic scans were performed by the same physician, who was aware of the patients' clinical history and who was blinded to the biopsy results and all imaging findings except those of US.

Ultrasonographic Technique

The ultrasonographic equipment used was a SSA-790A (Aplio XG; Toshiba Medical Systems Corp., Otawara, Japan). First, each lesion was scanned at baseline US. Each focal liver lesion was identified on baseline US and assigned a liver segment location according to Couinaud's (11) and Bismuth's (12) classification systems.

The contrast agent used in this study, NC100100, consists of perflubutane microbubbles surrounded by phospholipids.

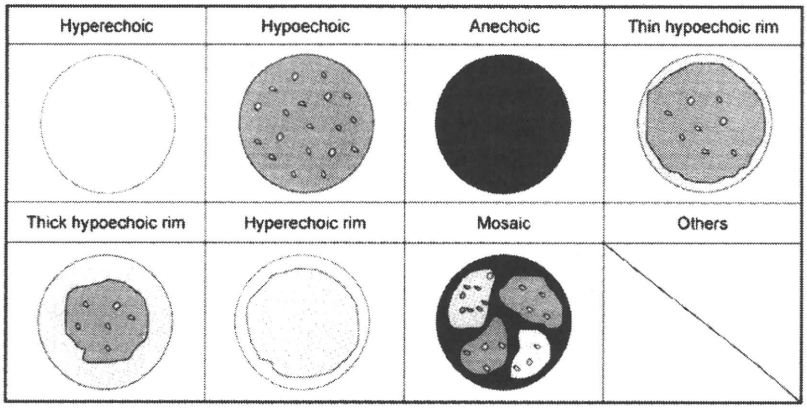

a.

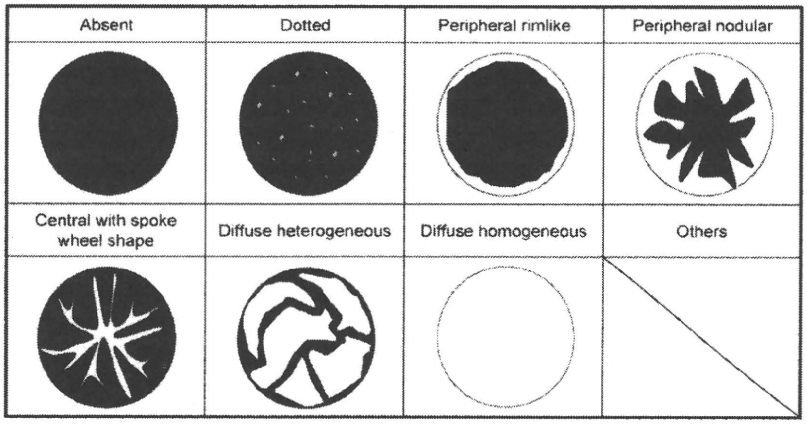

b.

Figure 1. (a) Illustration of morphologic patterns of hepatic tumors in the B-mode ultrasonography. (b) Illustration of enhancement patterns of hepatic tumors in the arterial phase.

The average diameter of the microbubbles is 2–3 μm. The contrast agent was injected as a 0.5 mL bolus into an antecubital vein with a 21-gauge peripheral intravenous cannula, followed by a 10 mL saline flush. The ultrasonographic equipment used was a SSA-790A with a 3.75-MHz convex transducer (PVT-375BT). The imaging mode was wideband harmonic imaging (commercially called Pulse subtraction) with transmission and reception frequencies of 3.75 and 7.5 MHz, respectively. When a suspected lesion was identified, a dynamic CEUS was performed with the focus depth beyond the region of interest, at a frame rate of 15 frames/s and a dynamic range of 45 dB. The mechanical index values were between 0.2 and 0.3, so that the microbubbles could be preserved throughout their half-life in microvessels and real-time exploration of the liver vasculature could be preserved. The region of interest was observed continuously for about 3 minutes from the time of injection (observation of the vascular phase). After 3 minutes, we froze the scan. Approximately 10 minutes after injection of the contrast agent to allow pooling of the agent in the hepatic parenchyma, we observed the tumors for enhancement using a sweep scan (observation of the delayed phase). Digital cine clips were stored during baseline US scanning and during the arterial phase (ie, 10–40 seconds from the beginning of the injection of the contrast agent bolus), during the portal phase (ie, 50–90 seconds from the beginning of the injection), the late phase (ie, 100–180 seconds from the beginning of the injection), and the delayed phase (ie, 10 minutes from the beginning of the injection).

Observer study for Obtaining Subjective Classifications of Echogenic Patterns

Digital cine clips stored on a digital hard disk were reviewed by three readers independently on a PC (VGN-S94PS; SONY, Tokyo, Japan). The readers were physicians trained in the use and interpretation of contrast agents in the liver. They were not involved in the ultrasonographic scanning and were

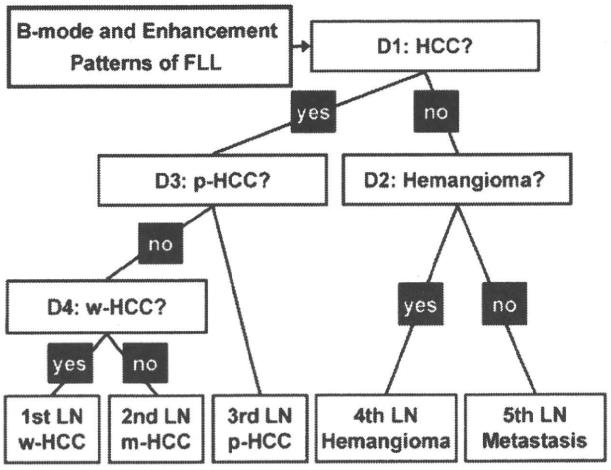

Figure 2. Illustration of the decision tree model used in this study. Four decision nodes in which alternative choice was determined by all five FLLs, leading to a final diagnostic decision for five liver lesions. D, decision node; FLL, focal liver lesion; HCC, hepatocellular carcinoma; LN, leaf node; m-HCC, moderately differentiated HCC; p-HCC, poorly differentiated HCC; w-HCC, well-differentiated HCC.

blinded to the identification, clinical histories, biopsy results, and other imaging findings of the patients. A clinical fellow in body imaging who was trained in contrast US, who neither scanned the patients nor was a reader, selected representative images and digital cine clips to show the baseline appearance as well as the arterial phase enhancement of the lesion. Cine clips were presented in a random order, and any identifying information was masked. In this study, we used only baseline and arterial-phase images.

From the baseline ultrasonographic features of a single mass in only one image, the reviewers were requested to classify the echogenic patterns of the mass into one of the following eight patterns: 1) hyperechoic; 2) hypoechoic; 3) anechoic with posterior echo enhancement; 4) thin hypoechoic rim; 5) thick irregular hypoechoic rim (bull's eye); 6) echogenic rim; 7) mosaic; and 8) others (Fig 1a). These patterns were proposed by Itai et al (13) for describing the characteristics of FLLs on baseline US.

After the ratings of echogenic patters of FLLs on the baseline US, the readers were asked to classify the contrast enhancement pattern of FLLs into one of the following eight patterns: 1) absent; 2) dotted; 3) peripheral rimlike; 4) peripheral nodular; 5) central with spoke wheel shape; 6) diffuse homogeneous; 7) diffuse heterogeneous; and 8) others (Fig 1b), which were proposed by Quaia et al (14). The readers were not asked to provide a diagnosis of an FLL in this observer study.

For employing these subjective ratings obtained by three readers classifying 137 FLLs using a computerized scheme, we created a matrix of 137 FLLs and 16 patterns, which indicated the total number of readers who rated the lesions for each pattern.

Computer-aided Diagnostic Scheme for the Classification of FLLs

To classify five types of FLLs (eg, well-differentiated, moderately differentiated, poorly differentiated HCC, liver metastasis, and liver hemangioma) in this CAD scheme, we employed four artificial neural networks (ANNs) as shown in Figure 2. ANNs are mathematical models based on biologic neural networks. These consist of an interconnected group of artificial neurons and processes information using a connectionist approach to computation. The order of the four decisions (labeled D1–D4) at each ANN was determined based on the diagnostic difficulties based on the physicians' knowledge. The four decisions used in this study were as follows:

D1: Is this lesion a HCC (yes) or other (no)?
D2: Is this lesion a hemangioma (yes) or metastasis (no)?
D3: Is this lesion a poorly differentiated HCC (yes) or other HCC (no)?
D4: Is this lesion a well-differentiated HCC (yes) or a moderately differentiated HCC (no)?

All decisions were determined using each of the ANNs in terms of a two-alternative choice method. In all of the four ANNs, we used 14 input units corresponding to each of seven patterns of subjective classification data in the matrix as described previously, and one image feature of the effective diameter of an FLL. We did not use one of the subjective classifications (others), because we assumed that these uncertain data might have a detrimental effect on the training of the ANNs. The effective diameter was calculated from a contour of an FLL, which was provided by a physician (K.S.).

We used the same parameter settings for the four ANNs, such as one hidden layer, eight hidden units, one output unit, 0.05 for the learning rate, and 0.30 for the slope of the sigmoid function except for the numbers of iterations for learning (15,16). The four ANNs were trained and tested independently by use of a leave-one-lesion-out test method. The range of iteration numbers between 200 and 600 with intervals of 100 were examined independently by monitoring of the accuracy in distinguishing between two groups for each ANN. Finally, we determined the number of iterations, such as 200 for D1 and D2, 400 for D3, and 600 for D4.

The correct classification of the CAD scheme for the five types of FLLs was determined when the final outcome from the four ANNs agreed with the "gold standard." The classification accuracies for each type of FLL and also for all 137 FLLs were determined with percentages of correctly classified cases among the total number of cases.

Table 1
The Total Number of Lesions Rated by Three Readers for Subjective Classification of Eight Ultrasonographic Patterns of B-mode Imaging

		Classification by Three Readers															
Lesion	Number of Lesions	Hyperechoic		Hypoechoic		Anechoic		Thin Hypoechoic Rim		Thick Hypoechoic Rim		Hyperechoic Rim		Mosaic		Others	
HCC	74	18	(8%)	92	(41%)	0	(0%)	50	(23%)	4	(2%)	3	(1%)	44	(20%)	11	(5%)
w-HCC	23	2	(3%)	42	(61%)	0	(0%)	9	(13%)	1	(1%)	1	(1%)	11	(16%)	3	(4%)
m-HCC	36	11	(10%)	42	(39%)	0	(0%)	29	(27%)	2	(2%)	1	(1%)	17	(16%)	6	(6%)
p-HCC	15	5	(11%)	8	(18%)	0	(0%)	12	(27%)	1	(2%)	1	(2%)	16	(36%)	2	(4%)
Metastasis	33	16	(14%)	24	(24%)	2	(2%)	5	(5%)	42	(42%)	0	(0%)	3	(3%)	7	(7%)
Hemangioma	30	37	(41%)	27	(30%)	0	(0%)	2	(2%)	0	(0%)	22	(24%)	2	(2%)	0	(0%)

Note. Numbers in parentheses are the percentage for the mean number of readers who rated the lesions for each pattern.
m-HCC, moderately differentiated hepatocellular carcinoma; p-HCC, poorly differentiated hepatocellular carcinoma; w-HCC, well-differentiated hepatocellular carcinoma.

Table 2
The Total Number of Lesions Rated by Three Readers for Subjective Classification of Eight Ultrasonographic Patterns of Contrast Harmonic Imaging

		Classification by Three Readers															
Lesion	Number of Lesions	Absent		Dotted		Peripheral Rimlike		Peripheral Nodular		Central with Spoke Wheel Shape		Diffuse Homogeneous		Diffuse Heterogeneous		Others	
HCC	74	0	(0%)	0	(0%)	2	(1%)	19	(9%)	0	(0%)	104	(47%)	97	(44%)	0	(0%)
w-HCC	23	0	(0%)	0	(0%)	0	(0%)	2	(3%)	0	(0%)	34	(49%)	33	(48%)	0	(0%)
m-HCC	36	0	(0%)	0	(0%)	1	(1%)	6	(6%)	0	(0%)	69	(64%)	32	(30%)	0	(0%)
p-HCC	15	0	(0%)	0	(0%)	1	(2%)	11	(24%)	0	(0%)	1	(2%)	32	(71%)	0	(0%)
Metastasis	33	0	(0%)	0	(0%)	28	(28%)	40	(40%)	2	(2%)	1	(1%)	28	(28%)	0	(0%)
Hemangioma	30	0	(0%)	0	(0%)	45	(50%)	43	(48%)	0	(0%)	2	(2%)	0	(0%)	0	(0%)

Note. Numbers in parentheses are the percentage for the mean number of readers who rated the lesions for each pattern.
m-HCC, moderately differentiated hepatocellular carcinoma; p-HCC, poorly differentiated hepatocellular carcinoma; w-HCC, well-differentiated hepatocellular carcinoma.

RESULTS

Table 1 shows the distribution of morphologic patterns of the hepatic tumors as rated by three readers on baseline US. The following are the approximate average numbers of the type of lesions rated by the three readers. The results indicated that 30 (41%) of the 74 HCCs were visualized as having a hypoechoic pattern; 14 (42%) of the 33 liver metastases were visualized as having a thick, irregular hypoechoic rim pattern; 12 (41%) of the 30 hemangiomas had a hyperechoic pattern; 14 (61%) of the 23 well-differentiated HCCs; 14 (39%) of the 36 moderately differentiated HCCs were classified as having a hypoechoic pattern; and 5 (36%) of 15 the poorly differentiated HCCs were classified as having a mosaic pattern.

Table 2 shows the distribution of enhancement patterns of the hepatic tumors as rated by the three readers on CEUS. In the arterial phase, 67 (91%) of the 74 HCCs exhibited a homogeneous or heterogeneous pattern of enhancement; 35 (47%) exhibited a homogeneous pattern and 33 (44%) exhibited a heterogeneous pattern; 13 (40%) of the 33 liver metastases exhibited a peripheral nodular pattern of enhancement; 15 (50%) of the 30 liver hemangiomas exhibited a peripheral rimlike pattern of enhancement; 22 (97%) of the 23 well-differentiated HCCs exhibited a homogeneous or heterogeneous pattern of enhancement; 12 (49%) exhibited a homogeneous pattern and 11 (48%) exhibited a heterogeneous pattern; 23 (64%) of the 36 moderately differentiated HCCs exhibited a homogeneous pattern of enhancement; and 11 (71%) of the 15 poorly differentiated HCCs exhibited a heterogeneous pattern of enhancement.

The computer performance in terms of the number of FLLs correctly classified and the classification accuracies (%) in each of the four ANNs were 133 of 137 (97.1%) for

Table 3
Performance of CAD Scheme for Classification in Five Categories Using Physicians' Subjective Pattern Classification

		Classification with CAD									
		HCC									
Lesion	Number of Lesions	w-HCC		m-HCC		p-HCC		Metastasis		Hemangioma	
HCC	74										
w-HCC	23	15	(65.2%)	4	(17.4%)	4	(17.4%)	0	(0.0%)	0	(0.0%)
m-HCC	36	16	(44.4%)	15	(41.7%)	5	(13.9%)	0	(0.0%	1	(2.7%)
p-HCC	15	1	(6.7%)	1	(6.7%)	12	(80.0%)	1	(6.7%)	0	(0.0%)
Metastasis	33	1	(3.0%)	0	(0.0%)	1	(3.0%)	28	(84.8%)	3	(9.1%)
Hemangioma	30	0	(0.0%)	0	(0.0%)	1	(3.3%)	1	(3.3%)	28	(93.3%)

CAD, computed-aided diagnosis; m-HCC, moderately differentiated hepatocellular carcinoma; p-HCC, poorly differentiated hepatocellular carcinoma; w-HCC, well-differentiated hepatocellular carcinoma.
Overall diagnostic accuracy: 98/137 (71.5 %).
CAD performance was evaluated by a leave-one-case-out method.

D1, 56 of 63 (88.9%) for D2, 62 of 74 (83.9%) for D3, and 20 of 59 (66.1%) for D4. Table 3 shows the performance of the computerized scheme for the classification of the five types of FLLs. The classification accuracies for the 137 FLLs were 84.8% for metastasis, 93.3% for hemangioma, 65.2% for well-differentiated HCC, 41.7% for moderately differentiated HCC, and 80.0% for poorly differentiated HCC. When the classification was conducted only for three types of FLLs (HCCs, metastasis, and hemangioma), the classification accuracy for all HCCs was 98.6%, as shown in Table 4. The average classification accuracies for three and five types of FLLs were 94.2% and 71.5%, respectively.

Figures 3 to 7 show examples of baseline and contrast-enhanced ultrasonographic images for each of the five types of FLLs that were classified correctly by the CAD. The results in Table 3 indicated that eight FLLs were incorrectly classified by the CAD into three types of FLLs, which consisted of one HCC, five metastases, and two hemangiomas. The CAD incorrectly classified one HCC as a metastasis, five metastases as two HCCs and three hemangiomas, and two hemangiomas as one HCC and one metastasis. Therefore, the classification accuracies for malignant (HCCs and metastases) and for benign (hemangiomas) lesions were 94.4% and 93.3%, respectively.

DISCUSSION

The characterization of FLLs using state-of-the-art US includes a gray-scale morphologic evaluation coupled with vascular information derived from color or power Doppler US (17). The comparison of conventional US with contrast-enhanced CT and MRIs for characterization of liver masses, however, shows that US is generally inferior at this task (18–21).

Table 4
Performance of CAD Scheme for Classification in Three Categories Using Physicians' Subjective Pattern Classification

		Classification with CAD					
Lesion	Number of Lesions	HCC		Metastasis		Hemangioma	
HCC	74	73	(98.6%)	1	(1.4%)	0	(0.0%)
Metastasis	33	2	(6.1%)	28	(84.8%)	3	(9.1%)
Hemangioma	30	1	(3.3%)	1	(3.3%)	28	(93.3%)

CAD, computed-aided diagnosis; HCC, hepatocellular carcinoma.
Overall diagnostic accuracy: 129/137 (94.2 %).
CAD performance was evaluated by a leave-one-case out method.

The more recent introduction of second-generation ultrasonographic contrast agents such as DMP 115, BR 1, and NC100100, together with newer imaging techniques, has provided much better imaging capabilities. These agents may be imaged at a low mechanical index, thus preserving the microbubbles and allowing real-time and continuous imaging of both a lesion and its vessels. Among recent reports evaluating these second-generation ultrasonographic contrast agents, Quaia et al (14) demonstrated that the overall diagnostic accuracy in the discrimination between benign and malignant tumors of the liver by readers 1 and 2 was 49% and 51% before the use of a contrast agent and increased to 85% and 88% after the use of the contrast agent, respectively. In addition, Wilson et al (22) reported that the overall diagnostic accuracy with the use of their algorithm was 86% (25 of 29) in HCC, 73% (11 of 15) in non-HCC malignancy, 92% (24 of 26) in hemangioma, and 95% (19 of 20) in FNH. Their algorithm is designed primarily to classify the lesions according to the presence or absence of sustained enhancement

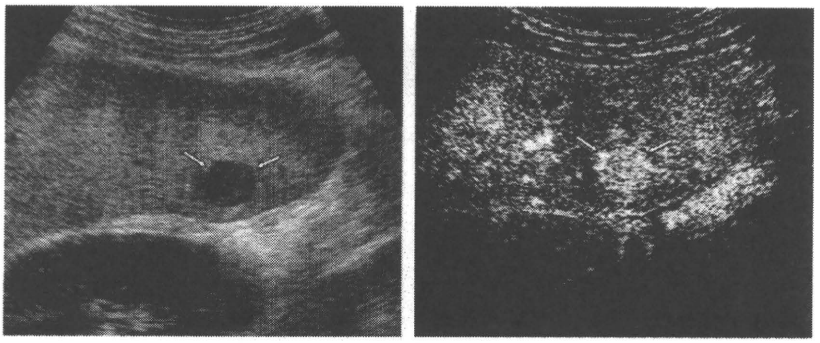

a. b.

Figure 3. A 28-year-old man with alcoholic cirrhosis and hepatocellular carcinoma *(arrows).* **(a)** Sagittal B-mode ultrasound shows hypoechoic mass *(arrows)* in right lobe of liver. **(b)** In arterial phase, lesion *(arrows)* shows diffuse homogeneous and slightly hypervascularity relative to liver parenchyma. Percutaneous biopsy revealed well-differentiated hepatocellular carcinoma.

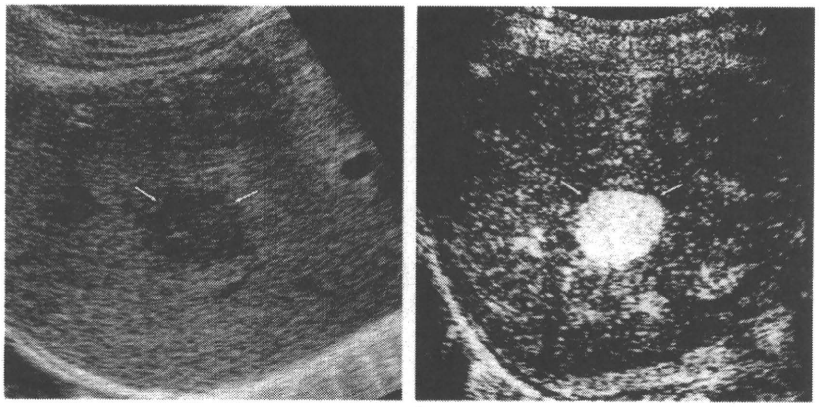

a. b.

Figure 4. A 73-year-old woman with hepatitis C cirrhosis and hepatocellular carcinoma *(arrows).* **(a)** Oblique subcostal B-mode ultrasound shows mass *(arrows)* with thin hypoechoic rim in right lobe of liver. **(b)** In arterial phase, the lesion *(arrows)* shows diffuse homogeneous and fairly hypervascularity relative to liver parenchyma. Percutaneous biopsy revealed moderately differentiated hepatocellular carcinoma.

in the extended portal phase. According to their classification, 48 (92%) of 52 benign lesions showed positive or sustained enhancement, and 41 (93%) of 44 malignancies showed negative enhancement or washout in the extended portal phase.

In our present study, to establish CAD for the diagnosis of FLLs, we used morphologic features as image features of hepatic tumors on baseline US and the contrast enhancement pattern in the arterial phase of contrast-enhanced US. However, we did not use findings from the portal, late, or delayed phase (ie, the presence or absence of washout) as image features of our CAD.

The diagnosis of hepatic tumors by baseline US is generally considered nonspecific. In fact, Itai et al (13) reported that the average diagnostic accuracy of hepatic tumors by baseline US was 68% in HCC, 77% in metastatic liver tumors, and 77% in hemangiomas. However, mosaic and hypoechoic patterns are findings that are relatively specific for HCC, and the sensitivity of mosaic and hypoechoic patterns is reported to be 91% and 92%, respectively. Therefore, we used baseline ultrasonographic images as the basis to establish CAD for the diagnosis of FLLs.

According to Jang et al (23), the dysmorphic vessels of HCC are distinctly different from the central stellate vessels demonstrated in FNH or peripheral nodular enhancement of hemangioma in the arterial phase. Therefore, the authors reported that a careful analysis of the vascular morphology during the wash-in of contrast material often contributes to

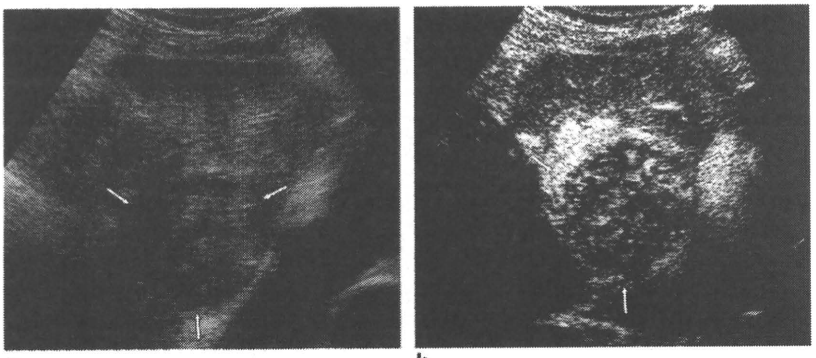

a. b.

Figure 5. A 75-year-old man with hepatitis C cirrhosis and hepatocellular carcinoma *(arrows)*. **(a)** Oblique subcostal left-lobe B-mode ultrasound shows mosaic mass *(arrows)*. **(b)** In the arterial phase, lesion *(arrows)* shows diffuse heterogeneous and slightly hypovascularity relative to liver parenchyma. Percutaneous biopsy revealed poorly differentiated hepatocellular carcinoma.

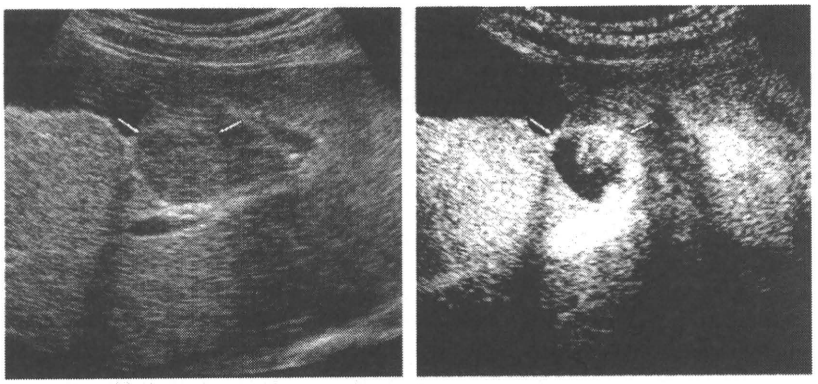

a. b.

Figure 6. A 38-year-old woman with liver hemangioma *(arrows)*. **(a)** Oblique subcostal B-mode ultrasound shows mass with hyperechoic rim *(arrows)*. **(b)** In the arterial phase, the image shows peripheral puddles of contrast that were enhanced more than the adjacent liver parenchyma.

the diagnosis of HCC and its differentiation from other benign tumors. Thus, the arterial phase is assumed to be one of the most important phases for the differential diagnosis of hepatic tumors. However, Wilson et al (22) and Quaia et al (14) reported that the presence or absence of washout in the portal phase and late phase (referred to as extended portal phase by Wilson et al) would be considered useful in the differential diagnosis of hepatic tumors, especially between benign and malignant tumors. The reason for our use of image findings only in the arterial phase as image features is as follows. In our present study, we used the reviewers' subjective data for CAD input data, although our future goal is to recognize the ultrasonographic image data automatically as input data to the CAD system. However, it is difficult to recognize automatically all of the data in a dynamic-imaging series for input data because of the problem of timing of patients' breath holding. We therefore used images only in the arterial phase, which is affected less by breathing.

According to the results of the pattern classification of baseline US, HCCs were most frequently classified into a hypoechoic pattern (41%), followed by a thin hypoechoic rim pattern (23%) and a mosaic pattern (20%). Makuuchi et al (24) described the mosaic pattern as architecture specific for HCC; this finding included 81% of HCCs ranging from 2 to 5 cm in diameter. However, the frequency of this finding obviously decreased as the size of the lesion decreased. It has been shown that, in lesions smaller than 2 cm, most HCCs appear as a hypoechoic mass on US (25). The average largest diameter of HCC in our study was 25 mm, which is relatively small, and therefore the hypoechoic pattern may be assumed to be the most common pattern of HCC.

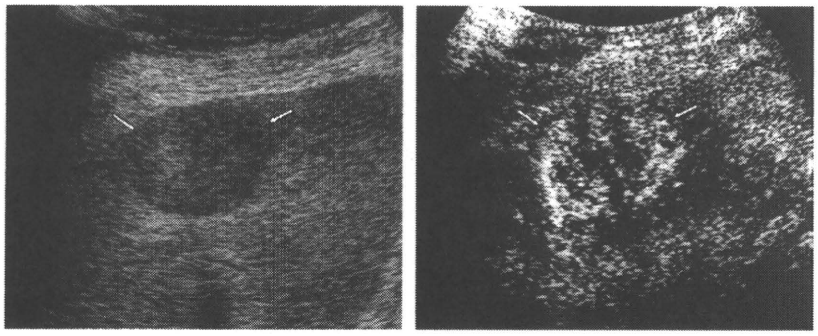

a. b.

Figure 7. A 65-year-old man with metastatic colon cancer *(arrows)*. **(a)** Intercostal B-mode ultrasound shows hypoechoic mass *(arrows)*. **(b)** In the arterial phase, lesion *(arrows)* shows marginal vascularity.

According to the degree of differentiation, there was a tendency that the ratio of the hypoechoic pattern gradually decreased from well-differentiated HCC to poorly differentiated HCC, whereas the thin hypoechoic rim pattern and mosaic pattern, generally specific for HCC, increased from well-differentiated to poorly differentiated HCC. The size of the HCC was assumed to contribute to this trend as well. On the other hand, according to the results of the contrast enhancement pattern of US, most HCCs were classified as diffuse homogeneous (47%) or diffuse heterogeneous patterns (44%).

When the enhancement patterns were examined in tumors other than HCC, including metastatic liver tumor and hemangioma, diffuse patterns were observed in 29% of metastatic liver tumors (most of them showed a diffuse heterogeneous pattern) and 2% of hemangiomas, thus suggesting that this finding would be useful for the differential diagnosis between HCC and other tumors. With regard to the degree of differentiation, 64% of moderately differentiated HCCs showed diffuse homogeneous patterns, whereas 71% and 24% of poorly differentiated HCCs showed diffuse heterogeneous patterns and peripheral nodular patterns, respectively. Thus, the blood distribution within the tumor tended to be more heterogenous in poorly differentiated HCC than in moderately or well-differentiated HCC. However, when the patterns of well-differentiated HCC were compared to those of moderately differentiated HCC, the ratio of a diffuse homogenous pattern to a diffuse heterogenous pattern was slightly lower in well-differentiated HCC than in moderately differentiated HCC, but there were also many nodules that showed similar patterns. Therefore, it is difficult to diagnose the differentiation of HCC even with the arterial-phase information obtained with CEUS.

Jang et al (23) reported that extended observation of the portal phase is helpful in making a correct diagnosis of HCC, because washout later than in the typical portal phase occurs slightly more frequently than does washout within 90 seconds, thus raising the possibility that careful monitoring of not only the arterial phase, but also a relatively late phase could further improve the diagnostic accuracy. Furthermore, newer software developed specifically for CEUS—particularly maximum-intensity-projection techniques—has the potential to improve the diagnostic accuracy in the histologic diagnosis of HCCs (26,27).

Metastatic liver tumors most frequently showed a thick, hypoechoic rim pattern in 42% on baseline US, but also showed various patterns including hypoechoic and hyperechoic patterns. On the other hand, in hemangioma, a hyperechoic pattern (41%) and thin hypoechoic rim pattern (24%), which are generally characteristic of hemangioma, were observed in many cases, but a hypoechoic pattern was also seen in 30%, suggesting that a differential diagnosis with baseline ultrasonographic imaging alone is difficult. However, the thin hypoechoic rim pattern and mosaic pattern, both of which are assumed to be characteristic of HCC, were scarcely observed in metastatic liver tumor and hemangioma and were thus considered useful in the differentiation of these tumors.

According to the classification by contrast enhancement pattern, both metastatic liver tumor and hemangioma tended to show peripheral rimlike and peripheral nodular patterns frequently. Quaia et al (14) reported that most hemangiomas (79%, 44/56) displayed a peripheral nodular pattern; the frequency was higher than that (48%) in our present study. The reason for this discrepancy may be that, although Quaia et al (14) monitored images not only in the arterial phase, but also in other phases in a continuous fashion, we evaluated images only in the arterial phase. In other words, it is possible that hemangioma with a very slow blood flow was diagnosed as having a peripheral rimlike pattern only in the arterial-phase image. Furthermore, it seemed difficult to differentiate between hypovascular-type metastatic liver tumor and hemangioma from images in the arterial phase alone. These may

contribute to the result of CAD analysis demonstrating that the diagnostic accuracy was very high in HCC (98.6%), but was relatively low in hemangioma (93.3%) and metastatic liver tumor (84.8%).

The principal limitation of this study was that almost all specimens for histopathologic diagnosis of the degree of differentiation of HCC were obtained by percutaneous biopsy. The specimens obtained by percutaneous biopsy allowed us to evaluate only a small part of the HCC lesion, which had been produced through a process called multistep hepatocarcinogenesis (ie, successive development of well-differentiated HCC from a dysplastic nodule through a dysplastic nodule with malignant foci), and consequently had histopathologic heterogeneity inside. However, surgical verification is obtained infrequently, especially in patients with HCC, because small HCC lesions are often treated with transcatheter arterial chemoembolization or percutaneous ablation, especially in cirrhotic patients whose functional reserve is severely impaired.

The second limitation is that FNH and hepatic adenoma were not included in this study. Both FNH and hepatic adenoma tend to have FLLs presenting a hypervascular pattern in the arterial phase, and it can be difficult to distinguish from HCC, metastatic liver tumor, and hemangioma. However, Kim et al (28) reported that monitoring the direction of early arterial filling or the vascular morphology continuously by CEUS enables one to differentiate, to some extent, among hepatic tumors with hypervascularity, including FNH, hemangioma, HCCs, or metastases. However, hepatic adenoma lacks characteristic features even with CEUS, and differentiation of hepatic adenoma from other plethoric FLLs has been reported to be difficult. However, hepatic adenoma is a very rare tumor in Japan, and therefore it seems extremely rare for this tumor to become a subject of differential diagnosis.

The third limitation is that current CAD does have information from the images itself rather than criteria that have to be provided subjectively by the physicians. It may be necessary to establish a CAD scheme that recognizes the US images itself automatically as input data. Moreover, to improve the accuracy of diagnosis for FLLs, it would be necessary to use information of not only arterial phase images but also other phase images in the future.

CONCLUSION

We developed a computerized scheme for the classification of focal liver lesions using physicians' subjective classification of echogenic patterns in baseline and contrast-enhanced US. This CAD scheme has the potential to improve the diagnostic accuracy for hepatic lesions, especially for HCC, liver metastasis, and liver hemangioma. However, the accuracy in the histologic differential diagnosis of HCC based on baseline US and CEUS is still limited.

ACKNOWLEDGEMENT

The authors are grateful to Ryo Metoki, MD, Yasuharu Imai, MD, and Liu Guang-Jian, MD, for participating as observers; and to Mrs. Elisabeth Lanzl for improving the manuscript.

REFERENCES

1. Laghi A, Iannaccone R, Rossi P, et al. Hepatocellular carcinoma: detection with triple-phase multi-detector row helical CT in patients with chronic hepatitis. Radiology 2003; 226:543–549.
2. Martin DR, Semelka RC. Imaging of benign and malignant focal liver lesions. Magn Reson Imaging Clin N Am 2001; 9:785–802.
3. Hussain SM, Semelka RC, Mitchell DG. MR imaging of hepatocellular carcinoma. Magn Reson Imaging Clin N Am 2002; 10:31–52.
4. Yamashita Y, Hatanaka Y, Yamamoto H, et al. Differential diagnosis of focal liver lesions: role of spin-echo and contrast-enhanced dynamic MR imaging. Radiology 1994; 193:59–65.
5. Burns PN, Wilson SR, Simpson DH. Pulse inversion imaging of liver blood flow: improved method for characterizing focal masses with microbubble contrast. Invest Radiol 2000; 35:58–71.
6. Harvey CJ, Blomley MJK, Eckersley RJ, et al. Hepatic malignancies: improved detection with pulse-inversion US in late phase of enhancement with SH U 508A-early experience. Radiology 2000; 216:903–908.
7. Huang-Wei C, Bleuzen A, Bourlier P, et al. Differential diagnosis of focal nodular hyperplasia with quantitative parametric analysis in contrast-enhanced sonography. Invest Radiol 2006; 41:363–368.
8. Doi K. Computer status and future potential of computer-aided diagnosis in medical imaging. Br J Radiol 2005; 78(Spec No 1):S3–S19.
9. Doi K. Computer-aided diagnosis in medical imaging: historical review, current status and future potential. Comput Med Imaging Graph 2007; 31:198–211.
10. International Working Party. Terminology of nodular hepatocellular lesions. Hepatology 1995; 22:983–993.
11. Couinaud C. Le foie: etsudes anatomiques et chirurgicales. Paris, France: Masson, 1957; 9–12.
12. Bismuth H. Surgical anatomy and anatomical surgery of the liver. World J Surg 1982; 6:3–8.
13. Itai Y, Ohtomo K, Ohnishi S, et al. Ultrasonography of small hepatic tumors. Radiat Med 1987; 5:14–19.
14. Quaia E, Calliada F, Betolotto M, et al. Characterization of focal liver lesions with contrast-specific US modes and a sulfur hexafluoride-filled microbubble contrast agent: diagnostic performance and confidence. Radiology 2004; 232:420–430.
15. Ashizawa K, MacMahon H, Ishida T, et al. Effect of an artificial neural network on radiologists' performance in the differential diagnosis of interstitial lung disease using chest radiographs. AJR Am J Roentgenol 1999; 172:1311–1315.
16. Abe H, Ashizawa K, Li F, et al. Artificial neural networks (ANNs) for differential diagnosis of interstitial lung disease: results of a simulation test with actual clinical cases. Acad Radiol 2004; 11:29–37.
17. De Gaetano AM, Barbaro B, Chiarla C, et al. The tissue characterization of focal liver lesions by color Doppler echography [in Italian]. Radiol Med (Torino) 1995; 89:453–463.
18. Snow JH Jr, Goldstein HM, Wallace S. Comparison of scintigraphy, sonography, and computed tomography in the evaluation of hepatic neoplasma. AJR Am J Roentgenol 1979; 132:915–918.
19. Becker-Gaab C, zur Nieden J, Sauer U, et al. Sonographic diagnosis of liver tumors: results of comparative studies of ultrasound, computerized tomography, laparoscopy, biopsy and scintigraphy in 413 patients [in German]. Digitale Bilddiagn 1987; 7:35–42.

20. Noone TC, Semelka RC, Chaney DM, et al. Abdominal imaging studies: comparison of diagnostic accuracies resulting from ultrasound, computed tomography, and magnetic resonance imaging in the same individual. Magn Reson Imaging 2004; 22:19–24.
21. Vlachos L, Trakadas S, Gouliamos A, et al. Comparative study between ultrasound, computed tomography, intra-arterial digital subtraction angiography, and magnetic resonance imaging in the differentiation of tumors of the liver. Gastrointest Radiol 1990; 15:102–106.
22. Wilson SR, Burns PN. An algorithm for the diagnosis of focal liver masses using microbubble contrast-enhanced pulse-inversion sonography. AJR Am J Roentgenol 2006; 186:1401–1412.
23. Jang HJ, Kim TK, Burns PN, et al. Enhancement patterns of hepatocellular carcinoma at contrast-enhanced US: comparison with histologic differentiation. Radiology 2007; 244:898–906.
24. Makuuchi M, Hasegawa H, Yamazaki S, et al. Ultrasonographic features of hepatocellular carcinoma under 5 cm in diameter: mosaic pattern of internal echo and posterior echo enhancement [in Japanese]. Acta Hepatol 1981; 22:1740.
25. Shinagawa T, Ohto M, Kimura K, et al. Diagnosis and clinical features of small hepatocellular carcinoma with emphasis on the utility of real-time ultrasonography. A study of 51 patients. Gastroenterology 1984; 86: 495–502.
26. Sugimoto K, Moriyasu F, Kamiyama N, et al. Analysis of morphological vascular changes of hepatocellular carcinoma by micro flow imaging using contrast-enhanced sonography. Hepatol Res 2008; 38: 790–799.
27. Shiraishi J, Sugimoto K, Moriyasu F, et al. Computer-aided diagnosis for the classification of focal liver lesions by use of contrast-enhanced ultrasonography. Med Phys 2008; 235:1734–1746.
28. Kim TK, Jang HJ, Burns PN, et al. Focal nodular hyperplasia and hepatic adenoma: differentiation with low-mechanical-index contrast-enhanced sonography. AJR Am J Roentgenol 2008; 190:58–66.